

## **Point Density Evaluation of Airborne LiDAR Datasets**

**Bojan Rupnik**

(University of Maribor, Maribor, Slovenia  
bojan.rupnik@um.si)

**Domen Mongus**

(University of Maribor, Maribor, Slovenia  
domen.mongus@um.si)

**Borut Žalik**

(University of Maribor, Maribor, Slovenia  
borut.zalik@um.si)

**Abstract:** Light Detection And Ranging (LiDAR) technology provides the means for fast and accurate acquisition of geospatial data. Quality control of the derived data is an important process for verifying whether the requirements of the scanning mission have been met. Point density presents one of the most important factors for evaluating LiDAR data. This paper presents a new method for evaluating the point density of LiDAR data through by applying methods of computational geometry. This method treats the LiDAR scan with regard to terrain characteristics and divides it into those areas that can be scanned and those that prevent quality scanning and produce weak returns. Point density evaluation is performed using the Voronoi diagram, which allows efficient extraction of actual LiDAR point density.

**Keywords:** LiDAR, Point density, Computational geometry, Voronoi diagram, Remote sensing, Quality control

**Categories:** I.3.5, I.3.8, J.7

## **1 Introduction**

### **1.1 LiDAR scanning**

Over the recent years, Light Detection and Ranging (LiDAR) has become one of the leading technologies in remote sensing. Mounted on airplanes, airborne LiDAR systems are capable of fast data acquisition from remote geographical areas. Other types include terrestrial scanning where LiDAR scanners can be stationary or mounted on land vehicles, however this paper is focused on data acquired by airborne scanning. Range measurement is performed by observing the time delay between the transmission and the detection of the laser pulse [Shan, 09]. In order to determine the position of the scanner, the global positioning system (GPS) is used, while the inertial measurement unit allows for determining the roll, pitch, and heading of the sensor mounted on the aircraft. This information, combined with the angular data measured by the scanning mechanism, is used to determine the georeferenced coordinates of the scanned points. Modern LiDAR scanners are capable of performing over 300,000 of

effective measurements per second [Massaro, 14] and ranging accuracy down to 5 mm [Deems, 13].

While the evaluation of LiDAR data is mainly focused on the vertical and horizontal accuracies of LiDAR points or inconsistencies from overlapping strips produced by multiple scanning [Habib, 10], there are other factors that have great influence on the quality of LiDAR data.

## 1.2 Point density significance and scanning issues

Point density, especially, has been recognised as one of the more important characteristics in mission planning [Maune, 03]. The effect of point density and point spacing on the accuracy of DTM generation has been studied by [Gueudet, 04, Liu, 07, Pirotti, 10, Sanii, 08]. These authors observed the accuracy of LiDAR-derived DTM by artificially reducing the point densities and compare them to the original scans. The effect of point density on DTM generation accuracy was also noticed by [Mongus, 12]. Although point density is recognised as an important factor, authors rarely provide methods for its estimation. The most obvious approach, often used in practice, is achieved by dividing the scan into cells and counting the number of points within them. While this approach offers a vague description of point density, it does not consider those variations in local point densities that appear due to various factors during scanning. Balsa-Barreiro et al. [Balsa-Barreiro, 12] studied the variations of point densities produced by an oscillating mirror scanning mechanism. This point density estimation was performed by dividing a single strip covering a terrain into several segments according to the scan angle. Comparison between the segments revealed an increase in point densities within the sectors where the scan angles are at the maximum. The authors suggested excluding extreme sectors for calculating the average point density. Alternative approaches for point density estimation that employ triangular meshes or Voronoi diagrams were suggested by [Shih, 06]. In their more recent research [Lari, 12] presented a method that considered planar relationships between neighbouring LiDAR points with focus of calculating point density of planar points. Local point densities are estimated by using a predefined number of nearest neighbours for each point per area of the circle between the point and the furthest of the selected neighbours. Their approach also provides suitable means for estimating the point densities in terrestrial LiDAR scans.

Problems arise when a pulse produces no return, which leads to voids in the data. Void appearances in LiDAR data occur due to several factors, most of which can be attributed to shadows and weak returns [Becker, 13]. Although the effects of both cases may be similar, distinguishing between shadows and weak returns allows for a better evaluation of LiDAR scans. Shadows are a consequence of objects blocking the path of the laser pulse and can be avoided or drastically reduced by multiple scanning. On the other hand, voids that appear due to weak returns are caused by terrain characteristics that prevent proper scanning. Weak returns are usually the result of the laser pulse hitting a surface, which reflects the majority of the pulse away from the scanner, and returns too small an amount of pulse energy for detection [Maune, 03]. Multiple scanning of such areas does not solve this problem, and thus it is viable to question whether they should be considered during point density estimation.

Minimal point density is a general requirement in the contract between the customer and the LiDAR operator, and presents one of the major influences on

variable mission costs [Saylam, 09]. The expected point density of LiDAR scanning is mainly dependent on mission plan parameters such as scan area, scan frequency, scan angle, pulse repetition frequency, scanning altitude, and aircraft speed. In the desire to set these parameters for minimising mission costs, quality control presents an important process for both parties to confirm as to whether the mission requirements have been met. This paper proposes a new method for LiDAR point density evaluation by taking into account those terrain areas that prevent effective scanning. LiDAR data evaluation focuses on areas that can be directly influenced by adhering to the mission plan, while those areas of weak returns that are the results of unfavourable terrain characteristics are excluded. Separation of weak return areas from successfully scanned areas reduces the bias in estimating the point density of scans covering unfavourable terrain characteristics such as rivers, lakes, etc.

## 2 Point Density Calculation

While point densities from LiDAR scans rely on several factors, a theoretical estimation is described by

$$\rho = F_n T_s / A \quad (1)$$

where  $F$  represents the scanning frequency,  $T_s$  the net flying time per strip,  $n$  the number of strips, and  $A$  the scanned area [Baltsavias, 99]. While this equation provides a vague estimation, the expected result may be very different from it, depending on terrain characteristics, weather conditions, navigational errors, etc. Furthermore, the number of LiDAR points may be further reduced by filtering, depending on the purpose of LiDAR scanning. In order to provide a more precise estimation of point densities within a LiDAR scan, the proposed method handles data voids that can appear during scanning due to those factors mentioned above. This method isolates areas of weak returns and focuses on estimating the point densities of the remaining areas. Point density is estimated by constructing a Voronoi diagram on LiDAR points and observing the areas of the Voronoi regions. The Voronoi diagram is also used for reconstruction of the scan boundary, and also for precise descriptions of void areas, that are retrieved by inserting artificial points into the Voronoi diagram. This method consists of the following steps:

- Voronoi diagram construction,
- Scan boundary reconstruction,
- Weak return void filling,
- Point density calculation using the Voronoi diagram

### 2.1 Void Description

In order to handle voids in LiDAR data, it is first necessary to describe them. In continuous data, a void can be considered as any discontinuity that appears. LiDAR points, however, being sampled at a specific scanning frequency are recorded irregularly. Given the nature of LiDAR scanning, it can be expected that the points

are recorded with almost constant spacing along the scan line, with variations at objects and vegetation borders. Assuming ideal scanning conditions (flat terrain, straight flight line, etc.) any deviation from the average point spacing would indicate the occurrence of a void. By observing scanned points, a void appears when the distance between two consecutively recorded points exceeds the average spacing by a certain value. However, given that no point is expected to appear within the average point spacing of another, it is reasonable to take this space into account as well.

It is for this purpose that an area of influence is constructed around each point in such a way that each point covers an area between the previously and subsequently recorded point. This area is defined as the union of half-distances between neighbouring points. Based on this, a void is no longer regarded as the complete distance between consecutively recorded points, thus exceeding the average spacing. Instead, the average spacing is subtracted from both edges to the neighbouring points, as given in Equation 2:

$$v = x \in X \mid P_{i-1} + \bar{d}/2 < x < P_i - \bar{d}/2 \quad (2)$$

where  $v$  indicates the covered length (area) of the void,  $X$  represents a line,  $\bar{d}$  the average point spacing of LiDAR points, and points  $P_{i-1}$  and  $P_i$  the points encompassing a void. An example of this idea can be seen in Figure 1.

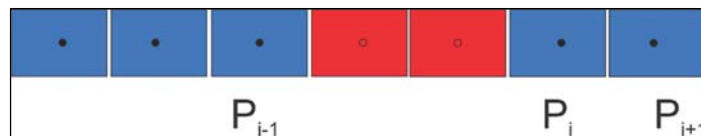


Figure 1: Void area (red) restricted by neighboring points

As it is, this approach is only suitable for describing voids on flat surfaces, which is hardly the only expected result of LiDAR scanning. Any change in the geometry that occurs by the appearances of objects or vegetation disrupts the linear pattern of the scanned points. This understanding requires a different approach to handling voids, although the main concept of limiting the voids based on point distribution in local neighbourhoods remains valid.

## 2.2 Detecting weak returns

As mentioned earlier, the proposed method treats voids caused by shadows and those caused by weak returns separately. By excluding areas of weak returns, such as rivers or lakes, the point density estimation is focused only on those terrain parts that allow effective scanning. While point spacing by itself provides little indication whether a void is caused by a shadow or a weak return, LiDAR scanning provides additional data along with position, which can be exploited for further analysis. For the purpose of this method the required input data must include the GPS time of recording along with positional information of each point. A strong correlation between the time and spatial position of each LiDAR point allows for void detection in the time domain, in which the changes in the scan pattern do not pose a problem.

Except on the edges of the scan line, scanning is usually performed at an almost constant frequency. The elapsed time or time-frames between consecutively scanned points are thus expected to be nearly identical with only minimal variations. Based on this, the time for each detected return can be predicted. In this way, the missing returns can be detected by finding a deviation from the predicted time. Although the shadows increase the time frames as well, their effect in comparison is minor enough to be ignored, which allows for distinguishing between both void types. The exception present the situations of weak return areas appearing within shadows, in which case a shadow may be falsely detected as part of the weak return area.

Identifying weak returns requires the defining of a tolerance for exceeding the expected time frame. Depending on the number and particularly the sizes of the voids within a scan, the mean time-frame between consecutively scanned points may significantly exceed the reasonably expected value therefore the median value is used instead. Similarly as in the geometrical description (Equation 2), a void can now be perceived in the time domain, which provides a significantly more reliable approach for detecting weak returns. This means that each point has to appear within its designated interval. The condition for identifying a weak return in a stream of LiDAR points, is given as follows:

$$t_{p_i} - t_{p_{i-1}} > 3\tilde{t}/2 \quad (3)$$

with  $t_{p_i}$  and  $t_{p_{i-1}}$  being the GPS times of consecutively scanned LiDAR points, and  $\tilde{t}$  the median value of all time frames. The median value is used instead of the mean, since weak returns can significantly increase the time between consecutively scanned points, and can thus influence the mean value. Regarding the correlation between the time and the position of the scanned points, the expected areas of influence are used for setting the maximum tolerance. Within the time domain, the area of influence of each point can be viewed as the time between  $t_p - \tilde{t}/2$  and  $t_p + \tilde{t}/2$  where the upper value corresponds with  $3\tilde{t}/2$  between two consecutively scanned points. This provides the same interval in the time domain as described in Figure 1 for the spatial domain for detection of voids.

Each pair of points encapsulating a void detected by this approach is marked for further processing. An example of weak return detection within a LiDAR dataset consisting of a river, vegetation, and several buildings is displayed in Figure 2. As it can be seen, the method outlines the points bordering on undetected water surfaces, while the shadows are unaffected. The red marked points represent those LiDAR points bordering on voids caused by weak returns. While water surfaces can produce returns, these are too dispersed compared to the rest of the scan to providing a proper representation of the scanned surface.

As already mentioned, the proposed approach relies on the correlation between the time and the position of consecutively scanned points. However, this correlation is disrupted whenever a sudden change in the geometry appears, such as the appearances of vegetation or objects. While objects present minor problems as the positional variations are usually relatively uniform along the objects borders, vegetation introduces substantial variations in the positions of the LiDAR points. This requires paying special attention to those void border points appearing in vegetation areas, such as trees or bushes on riverbanks.

Scanning a flat surface results in evenly-distributed points along the scan line. However, scanning vegetation or objects produces significant positional variations and breaks the linear distribution of consecutively scanned points. The result of this is a diminished correlation between the time of recording and the position of the scanned point, consequently the void border points detected during the time domain may not be properly reflected in the scan geometry. Void border points can be detected behind properly scanned points, thus preventing proper void description.

The distances between consecutively scanned points are observed in order to counter this effect. Any points found nearer between detected void borders along the scan-line, are used to replace the detected border points.

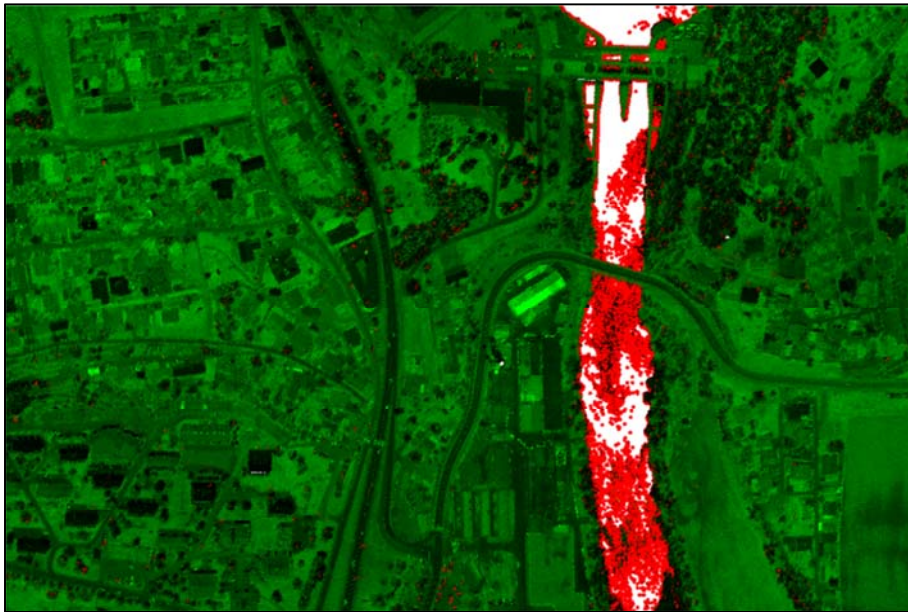


Figure 2: LiDAR points bordering on voids (red)

Figure 3 displays an example of proximity correction. The border points along the scan line are detected as too much time passed between consecutive returns ( $t_i, t_{i+1}$ ). While this represents a void in the time domain (left), the actual spatial representation requires that the borders are corrected remove any points appear within a void. This is done by replacing the border points with those that are geographically nearest (right).

Since the void border points in this approach are identified only per scan line appearance, it is necessary to examine the broader vicinity to completely describe the voids in local areas. The most straightforward approach would be to connect the neighbouring points into polygons and then subtract those polygons from the rest of the covered area. However, the arrangement of the void border points can lead to severe difficulties without a single solution. Among others, the unclear order of the points, concavities, possible holes within the polygons (caused by isolated validly

scanned points within a void), or voids running along the scanning direction, which may completely thwart the identification of a border.

A relationship between neighbouring points should be established to counter these problems. Constructing a Delaunay triangulation or its dual the Voronoi diagram provides a means of creating a quality mesh without unwanted elements [de Berg, 08].

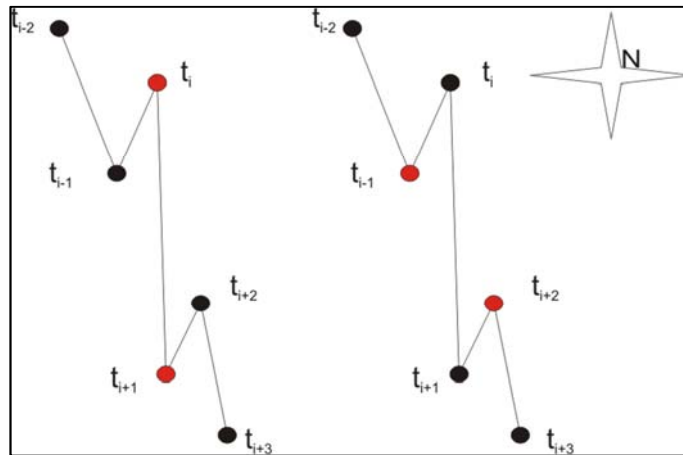


Figure 3: Proximity correction of void border points

### 2.3 The Voronoi diagram

While the use of Delaunay triangulations or Voronoi diagrams was suggested for point density estimation [Shih, 06], none of the solutions have suggested an approach for proper handling of data voids. The proposed method constructs the Voronoi diagram of a LiDAR dataset with regard to the weak return data voids, which improves the overall precision and reduces the bias of point density estimation caused by unfavourable terrain characteristics.

The previous section mentions the consideration of LiDAR points with regard to their areas of influence. While seen at the level of the scan-line this problem is 1-dimensional, parallels of this idea to the 2D Voronoi diagram are apparent. Although LiDAR points are provided with 3D positions among other data, only the x and y coordinates are used for constructing the Voronoi diagram. By using LiDAR points as sites of the Voronoi diagram, the Voronoi regions around the sites allow for computation of point density for each individual LiDAR point as the inverse area value of the Voronoi region. Disregarding data voids and other issues, the point density of a LiDAR dataset could be calculated by:

$$\rho = \frac{n}{\sum_{i=1}^n \text{Area}(R_i)} \quad (4)$$

where  $n$  represents the number of LiDAR points and  $R_i$  the Voronoi region of each point. While Equation 4 might provide a quick estimate of LiDAR point density by

subsequently subtracting the Voronoi regions constructed by void border points, there are two main problems that need to be addressed first.

Figure 4 displays a region of the Voronoi diagram constructed on the previously shown dataset (see Figure 2). The sites on the outer boundary of the dataset produce disproportionately large Voronoi regions, and are even unbounded at the sites that are part of the convex hull. Naturally, these regions cannot be used to represent the areas of influence of their corresponding LiDAR points, and need to be culled from the Voronoi diagram. Another issue is the handling of void borders. Just as each void border point was marked during void detection, so were their corresponding Voronoi regions. As explained in the continuation, simply removing those void regions is not sufficient for accurately describing weak return data voids.

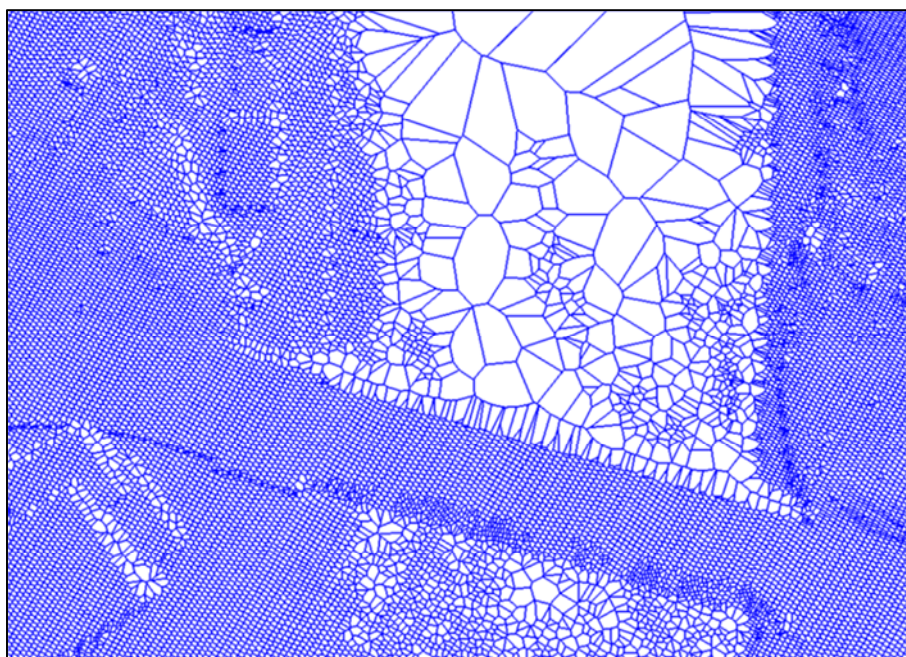


Figure 4: Voronoi diagram of LiDAR points from a region of the dataset displayed in figure 2

## 2.4 Boundary reconstruction

Along with culling the uncharacteristic Voronoi regions, the computation of the outer boundary is necessary to define the exact area covered by the LiDAR points. Assuming all outer points belong to the bounding rectangle, this process is trivial. However, if concavities appear on the outer boundary, they produce too large Voronoi regions within the bounding rectangle, and need to be addressed accordingly.

Although Delaunay triangulation-based methods for detecting the boundary points of point clouds do exist [Zalik, 06], those methods rely on the statistics of interior angles and edge lengths. Whilst this approach seems appropriate, and as an according

data structure is already given with the constructed Voronoi diagram, the z-shaped scanning pattern of the LiDAR points produced by the oscillating mirror scanning mechanism provides a possibility for constructing the exact boundary.

For this purpose the edges of the scan-lines are identified within the point cloud. While LiDAR points may carry the information as to whether they present the edge of a scan-line, this is marked by the LiDAR system and may not necessarily mark the real edge in the scanned geometry.

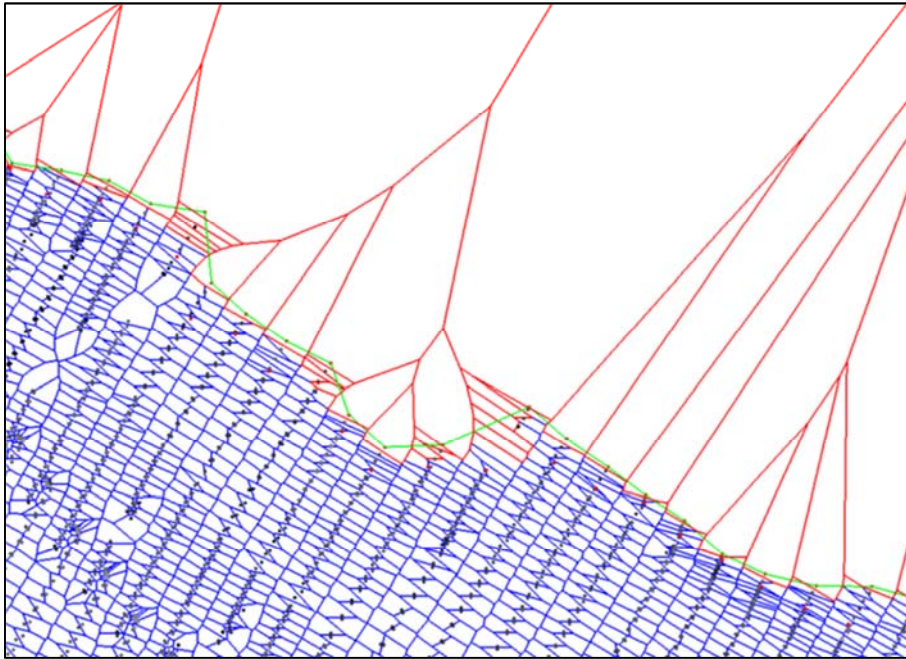


Figure 5: Boundary region culling

Therefore, it is necessary to check the points, as to whether they are the most extreme within a single swing. This is done by observing the distances between the starting point and the consecutively scanned points of the scan line. The distances increase until the furthest point is found, after which the distances begin to decrease. Since vegetation or objects may produce local variations of the calculated distances, it is necessary to use a frame of several points along the scan line to ensure that the most distant is found. The selected point is used as the base for finding the opposite extreme by continuing the approach. The opposite extremes are used to construct two separate polylines, representing the left and the right boundary of the point cloud along the flight direction. As for the top part of the boundary, the points between the beginning and the first extreme point are used.

In order to complete the frontal part of the boundary, the Voronoi neighbourhood of the starting point is checked for the nearest point of the scan line in the opposite direction, after which all points to the next extreme are used to construct the remainder of the starting boundary. The back side of the boundary is determined in

the same way using the finishing point and the last opposite extreme points. In order to deal with concavities, which represent the biggest problem of outer boundary reconstruction, each region of the Voronoi diagram is checked for intersection with the boundary polygon. All Voronoi regions intersecting the boundary polygon are culled from the Voronoi diagram, with the remaining regions covering the actual scanned area (Figure 5). In this way, all Voronoi regions that do not provide a suitable description in local areas of influence are removed.

## 2.5 Filling the voids

The Voronoi regions constructed around the void border sites (red points in Figure 6a) greatly deviate from the other regions in size. The straightforward approach suggests removing any region belonging to a border site. However, depending on the void geometry, a similar problem appears as with handling the outer boundary. Non-void points can produce overly large Voronoi regions (Figure 6b), which do not properly represent their local point density (Figure 6c). One of the reasons for this occurrence is the fact that every border point is not necessarily found during void detection. This is especially noticeable at concavities or in case where a void border runs parallel along the scanning direction, in which case a majority of the border may remain completely undetected.

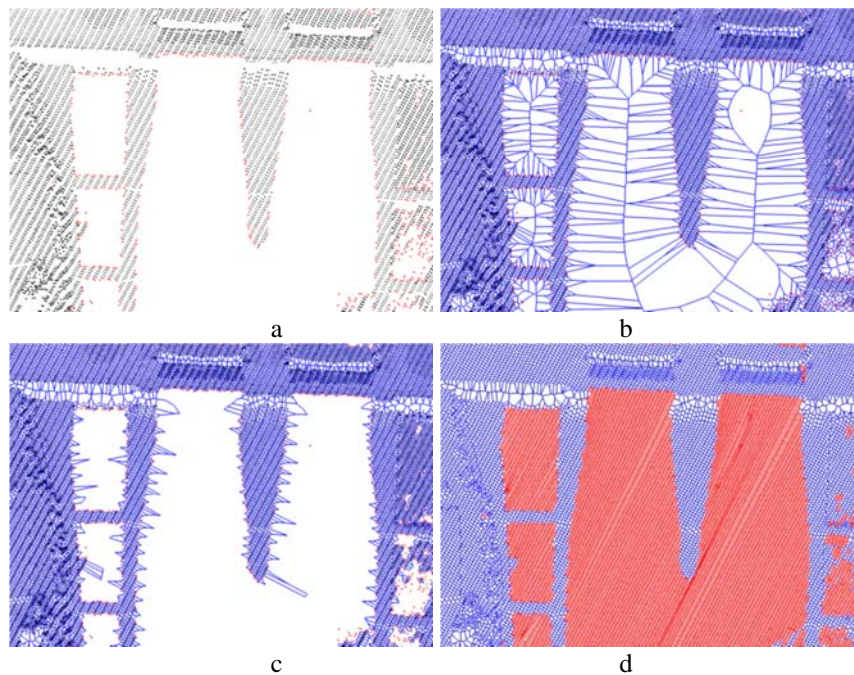


Figure 6: LiDAR weak return void borders (a), Voronoi diagram of the LiDAR dataset (b), Voronoi diagram with culled void regions (c), weak return void reconstruction (d)

Lines between the void border points are observed in order to address this problem. These lines are mostly aligned with the scan-line with minor variations. Based on the void definition with respect to the area of influence of neighbouring points, the solution requires bounding the void areas, while preserving the area of the scanned points. This cannot be done by simply removing the void border sites. Instead of this, the lines between void border points are used to predict the positions of weak return points. The points are predicted by linear interpolation between both void border points with the average distance between the last 10 consecutively scanned points. Artificial points calculated this way are used as additional input to the Voronoi diagram. The effect of inserting the artificial points becomes apparent, when observing the revised Voronoi regions (Figure 6d). The artificial points essentially fill those spots where the points were expected to appear, and thus expand the neighbouring Voronoi regions until they are bound by the actual void border sites. Consequently, it is no longer necessary to remove the void border sites from point density computation. Instead, the sites/regions constructed by the artificial points are used to describe weak return voids in the dataset.

At this stage the marked Voronoi regions offer a solid description of any weak return void. Essentially, it is now only necessary to remove any marked region from the Voronoi diagram, while the residue provides the basis for point density estimation.

## 2.6 Point density and point spacing

To sum it up, the proposed method includes the construction of a Voronoi diagram on a LiDAR dataset, after which all Voronoi regions belonging to the outer boundary and all regions covering weak return voids are removed. The point density of a LiDAR dataset is then:

$$\rho = \frac{n - n_b}{\sum Area(R_i) - \sum Area(R_v) - \sum Area(R_b)} \quad (5)$$

where  $n$  is the number of all sites of the Voronoi diagram prior to inserting artificial points, and  $n_b$  the number of sites on the boundary. Areas of outer boundary Voronoi regions ( $R_b$ ) and weak returns ( $R_v$ ) are subtracted from the whole area of the Voronoi diagram. Since the Voronoi diagram constructs regions for each point individually, this approach allows for a precise analysis of variations in point density within a dataset at the level of a single point. Point spacing provides another important factor of LiDAR data evaluation and is highly linked with point density [Raber, 03]. Point spacing is calculated through the neighbouring relationships constructed by the Voronoi diagram. Distances to its neighbouring sites are calculated for each Voronoi site with the average value representing local point spacing. Sites that are inserted during void filling are excluded from point spacing calculation.

## 2.6 Strip overlapping

LiDAR scanning is often performed multiple times in order to cover larger areas or to increase the point density of a particular area. The resulting multiple scans, that may overlap each other, require some additional handling. Boundary detection is first performed for each strip individually. The final boundary is formed as a union of the

boundary polygons of each strip. The boundary Voronoi region culling is no longer performed per strip, instead only the Voronoi regions intersecting the final boundary are removed. As for the computation of weak return areas, they are performed for each strip. The weak return void areas are calculated for each strip separately. Otherwise, the points are inserted into the Voronoi diagram without any restrictions.

### 3 Results

The method was implemented using C++ and the Boost Voronoi library [Boost, 14] for the construction of the Voronoi diagram. The system consists of Intel Core 2 Q6600 CPU running at 2.4 GHz and 8GB of working memory. Datasets of various terrain types were selected for testing including at, hilly, urban, and vegetation areas. Most of the selected datasets include multiples of weak return areas (rivers, lakes, or ponds) in order to demonstrate the effect of limiting the point density calculation to the well-scanned surface. With LiDAR systems being capable of detecting multiple returns per pulse, only the last returns were used for the calculations, as they presented the highest probability of representing ground points. Strip overlapping is present in most of the datasets. The calculations included the complete area (boundary) of the scan, the number of detected weak returns, the estimated area covered by weak returns (artificially inserted Voronoi sites), average point spacing, and average point density. The weak return Voronoi regions were excluded from the point density and point spacing calculations. The results of the measurements can be seen in Table 1, and Figure 7 displays point density maps of some of the datasets.

Set	Points (M)	Strips	WR (K)	Area (km <sup>2</sup> )	Point spacing (m)	Point density (points /m <sup>2</sup> )	St. dev. (points /m <sup>2</sup> )
1	1.6	3	120	0.373	0.493	6.863	5.695
2	1.2	7	176	0.110	0.250	17.362	15.447
3	2.4	3	10	0.974	0.782	2.965	1.341
4	4.5	3	341	0.434	0.210	12.523	10.925
5	5.5	6	17	1.050	0.479	7.954	5.403
6	5.6	7	459	6.696	1.002	0.936	0.354

Table 1: Results of LiDAR point density estimation on test datasets

By discarding areas of weak returns and focusing the calculations only on properly scanned areas, the average point density is higher compared to the count per area. The relatively high standard deviation from the average value is mostly the

result of overlapping strips, which introduce great variations at overlapping areas. Otherwise, variations in point densities can be contributed to objects and vegetation, and also to the local density increases at the edges of the scan-line.

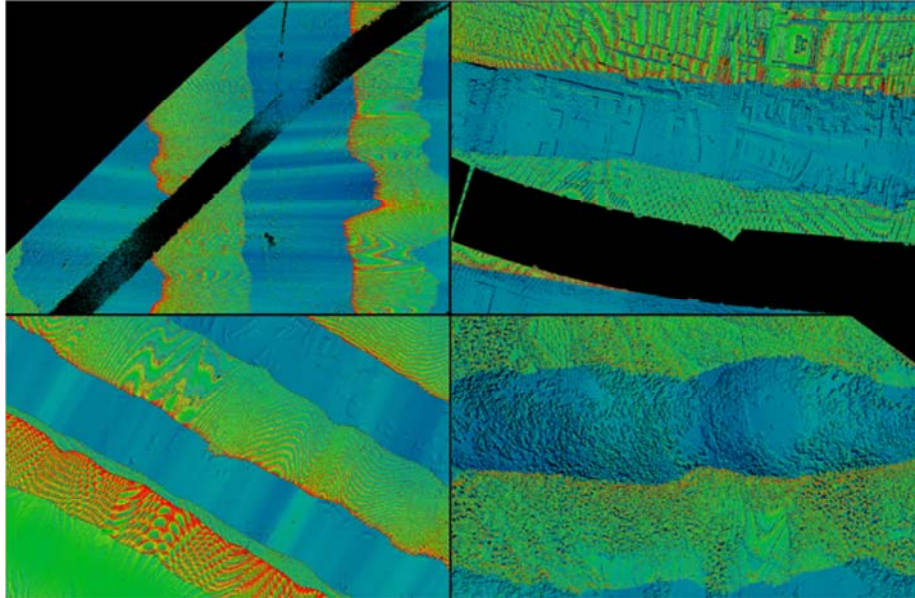
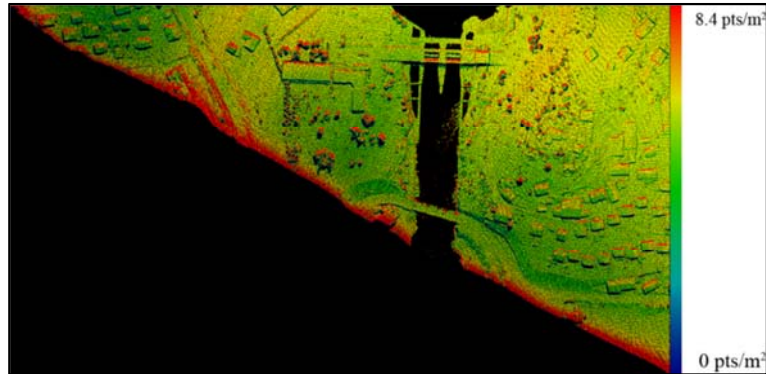
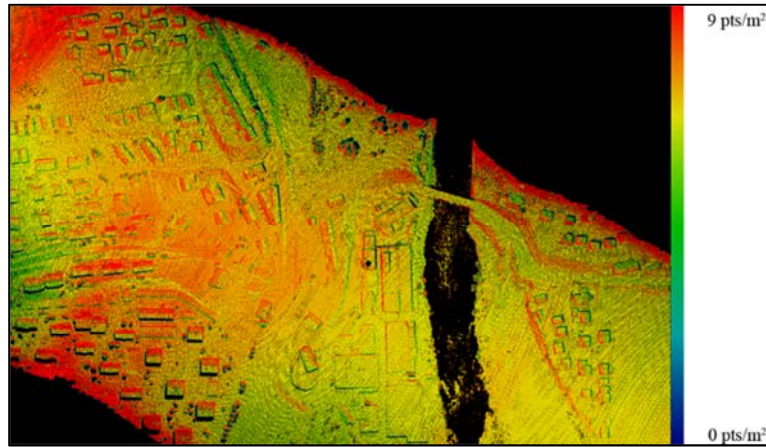
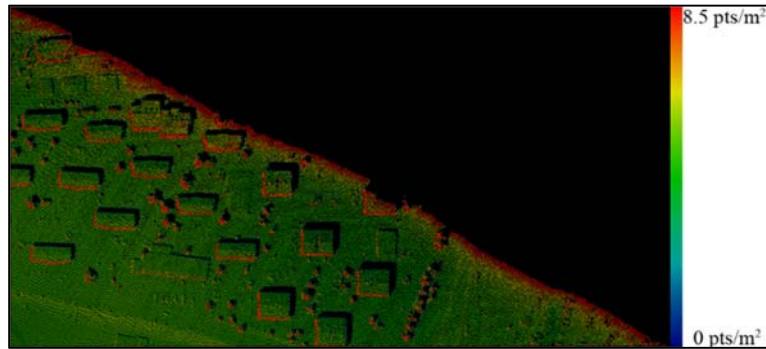


Figure 7: Point density maps of LiDAR datasets 1, 2, 3, and 4

A more detailed analysis was performed on Dataset 1 from Table 1. This dataset consists of a mainly at area with some vegetation cover and objects, a minor elevation and a river (Figures 8a to 8e). Strip overlapping covers approximately a quarter of the whole area. Observing the values per each strip individually reveals a more even distribution of point densities. Figures 8a, 8b, and 8c display the density maps of each individual strip. Different colour scales were used for each strip to emphasise variations in local point densities. Density build-ups can be seen at objects and vegetation appearances where they are oriented towards the scanner as well as at the edges of the scan-line. Decreased density areas can be seen around the shadows. The point densities at the river borders are not lowered by the weak return voids instead the values represent the point densities of local neighbourhoods. Figure 8d represents the point density including strip overlapping consisting of only last returns. Although only single pulse returns are usually used for LiDAR processing, the effect of using both first and last returns on point density was observed in Figure 8e to provide a better estimation in vegetation areas.

The resulting point densities of Dataset 1 can be seen in Table 2. Performing calculations per each strip individually, reveals a lower standard deviation compared to the results in Table 1. The higher standard deviation of the third strip is caused by a relatively small scanned area containing several shadows. Strip overlapping naturally produces an increase in point density. The overlapping strip areas (rows 4 and 5 of Table 2) can be seen in Figures 8d and 8e. The last row represents the values of

dataset 1 including both the first and last returns in order to properly estimate the point densities in vegetation areas.

*a**b**c*

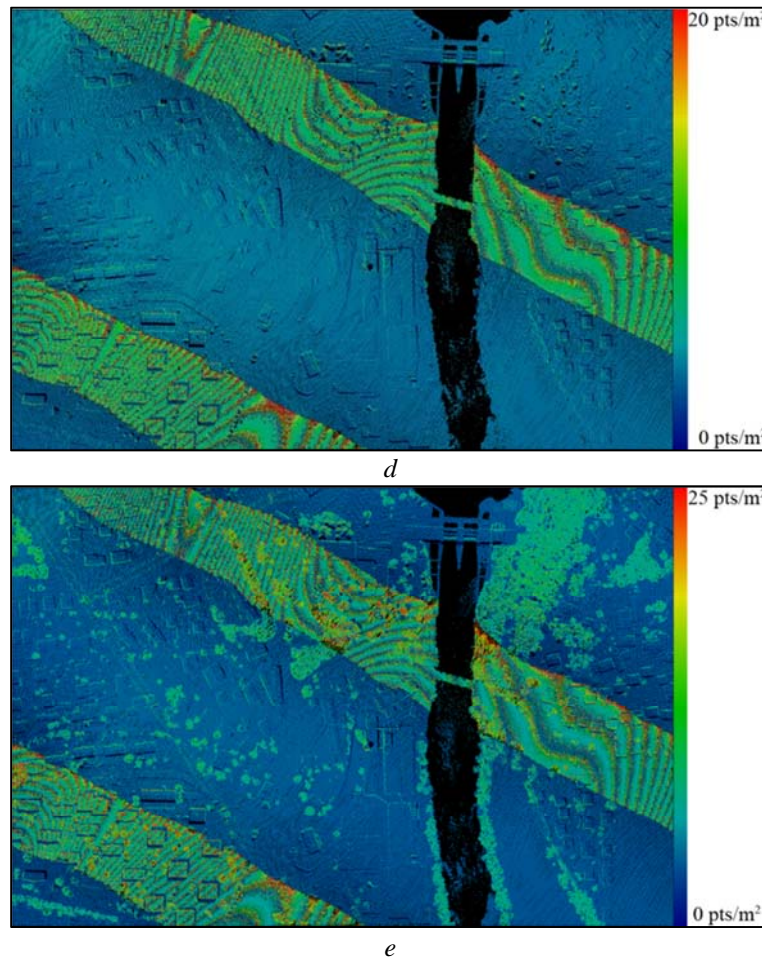


Figure 8: LiDAR point density maps of individual strips (a-c) and strip overlapping (d and e)

Each of the point density maps in Figure 8 is assigned a colour scale going from the blue shade representing the lowest point density and up to the highest point density represented by the red colour as displayed on the right side of each density map. While the calculations themselves reveal the average values and the standard deviations imply the differences, the density maps reveal the behaviour of the scanning. Overall the scans of the available datasets present a relatively equally distributed point density when observing last returns, while including other returns naturally increases point density as well as its variation. Further, the density maps reveal that each object creates a fairly characteristic variation in local point densities that could be used for further processing.

Strip	Points (M)	Area (km <sup>2</sup> )	WR (K)	Point spacing (m)	Point density (points/m <sup>2</sup> )	St. dev.
1	0.457	0.136	58	0.589	4.080	1.541
2	1.035	0.281	84	0.573	4.213	1.598
3	0.149	0.040	2	0.594	4.572	3.961
1-2	0.490	0.050	35	0.394	10.212	5.423
2-3	0.375	0.033	4	0.411	9.832	4.322
All	1.92	0.373	120	0.449	8.324	7.199

Table 2: Results of LiDAR point density calculation on dataset 1 per individual strip

## 4 Conclusion

The presented method is based on separating the terrain into valid and invalid areas, where invalid areas present terrain parts that do not to yield proper returns for LiDAR detection. While most of the weak return areas can be contributed to bodies of water, weak returns caused by other factors can be treated in the same way without noticeably reducing the quality of the method. Utilizing the Voronoi diagram provides means for measuring variations in point density with great precision at the level of each individual point. The number of detected weak returns and the cumulative areas of the Voronoi regions constructed by inserting artificial points provide an important measure for LiDAR data evaluation that needs to be considered along with point density and point spacing. Excluding weak return areas eliminates the disproportionate lowering of point densities that cannot be prevented, while flaws in point densities that occur due to inadequate mission planning are still detected, which provides an unbiased means for point density evaluation of LiDAR data.

The approach using the Voronoi diagram greatly increases the precision of point density evaluation compared to other methods, and at the same avoids errors that occur due to surfaces that cannot be scanned. As the point density maps reveal characteristic increases in point density at occurrences of objects, this method could be expanded for detection and reconstruction of objects from LiDAR scans.

### Acknowledgements

This work was supported by the Slovenian Research Agency under Grants L2-3650 and P2-0041.

### References

- [Balsa-Barreiro, 12] Balsa-Barreiro, J., Avariento, J. P., and Lerma, J.L.: Airborne light detection and ranging (lidar) point density analysis. *Scientific Research and Essays*, 7(33):3010-3019, 2012.
- [Baltsavias, 99] Baltsavias, E.P.: Airborne laser scanning: basic relations and formulas. *ISPRS Journal of Photogrammetry & Remote Sensing*, 54:199-214, 1999.

- [Becker, 13] Becker, J., Stewart, C., and Radke, R.J.: Lidar inpainting from a single image. In International Workshop on 3-D Digital Imaging and Modeling (3DIM), 2009.
- [Boost, 14] Boost.polygon voronoi library. <http://www.boost.org>, 2014.
- [de Berg, 08] de Berg, M., Cheong, O.: Computational Geometry: Algorithms and Applications Third Edition. Springer, 2008.
- [Deems, 13] Deems, J.S., Painter T. H., Finnegan, D.C.: Lidar measurement of snow depth: a review. *Journal of Glaciology*, Vol. 59(215), 2013
- [Gueudet, 04] Gueudet, Wells, Maidment, and Neuenschwander: Influence of the post-spacing density of the lidar-derived DEM on flood modeling. In Proceedings of the 2004 American Water Resources Association Spring Conference, 2004.
- [Habib, 10] Habib, A., Kersting, A.P., Bang, Ki In, and Lee Dong-Cheon: Alternative methodologies for the internal quality control of parallel lidar strips. In *IEEE Transactions on Geoscience and Remote Sensing*, volume 48, pages 221-236, 2010.
- [Lari, 12] Lari, Z. and Habib, A: Alternative methodologies for the estimation of local point density index: Moving towards adaptive lidar data processing. In *International Archives of the Photogrammetry, Remote Sensing and Spatial Information Sciences*, volume XXXIX-B3, 2012.
- [Liu, 07] Liu, X., Zhang, Z., Peterson, J., and Chandra, S.: The effect of lidar data density on DEM accuracy. In *MODSIM07: International Congress on Modelling and Simulation: Land, Water and Environmental Management: Integrated Systems for Sustainability*, pages 10-13, 2007.
- [Massaro, 14] R. D. Massaro, J. E. Anderson, J. D. Nelson, J. D. Edwards. A comparative study between frequency-modulated continuous Wave LADAR and linear mode LIDAR. *The International Archives of the Photogrammetry, Remote Sensing and Spatial Information Sciences*, Vol: XL-1, 2014.
- [Maune, 03] Maune, D. F.: Fema's mapping and surveying guidelines and specifications. In Proceedings of the Fall 2003 Conference of the American Society for Photogrammetry&Remote Sensing, 2003.
- [Mongus, 12]Mongus, D. , Žalik, B.: Parameter-free ground filtering of lidar data for automatic DTM generation. *ISPRS Journal of Photogrammetry and Remote Sensing*,66:1-12, 2012.
- [Pirotti, 10] Pirotti F., Tarolli, P.: Suitability of LiDAR point density and derived landform curvature maps for channel network extraction. *Hydrological Processes*, (24):1187-1197, 2010.
- [Shih, 06] Shih P.T, Huang, C.M.: Abstract, airborne lidar point cloud density indices (abstract). American Geophysical Union, Fall Meeting. 2006.
- [Raber, 03] Raber G.: The effect of lidar posting density on DEM accuracy and flood extent delineation. In Proceedings of the UCGIS Summer Assembly, 2003.
- [Sanii, 08] Sanii S.: Assessing the effect of point density and terrain complexity on the quality of lidar-derived dems in multiple resolutions. Master's thesis, University of Calgary, 2008.
- [Saylam, 09] Saylam, K.: Quality assurance of lidar systems mission planning. In *ASPRS Baltimore 2009 Conference Proceedings*, 2009.
- [Shan, 09] Shan, J., Toth, C.K.: Topographic Laser Ranging and Scanning: Principles and Processing. Taylor & Francis, 2009.
- [Žalik, 06] Žalik, B., Kolingerova, I.: Reconstructing domain boundaries within a given set of points using delaunay triangulation. *Computers and Geosciences*, 32:1310-1319, 2006.